Bio-Design and Manufacturing (2025) 8:835–846
https://doi.org/10.1631/bdm.2500046

RESEARCH ARTICLE

Design–simulation–manufacturing–assessment framework for geometric optimization of polymeric heart valves toward enhanced durability

Tianle Xu[1] · Zihan Zhu[2] · Yunhan Cai[1] · Shunping Chen[2] · Jia Guo[2] · Shengzhang Wang[1,3]

Received: 5 February 2025 / Accepted: 12 April 2025 / Published online: 9 September 2025

Abstract

Owing to their excellent biocompatibility and potential for durability enhancement, polymeric heart valves (PHVs) are emerging as a promising alternative to traditional prostheses. Unlike conventional materials, PHVs can be manufactured under precise design criteria, enabling targeted performance improvements. This study introduces a geometric optimization strategy for enhancing the durability of PHVs. The finite element method (FEM) is combined with a dip-molding technique to develop a novel polymeric aortic valve with improved mechanical properties. The tri-leaflet geometry is parameterized using B-spline curves, and the maximum stress in the valve is reduced from 2.4802 to 1.7773 MPa using a multiobjective optimization algorithm NSGA-II (non-dominated sorting genetic algorithm II). Pre-optimized and optimized valve prototypes were fabricated via dip-molding and evaluated during pulsatile-flow tests and accelerated wear tests. The optimized design meets the ISO 5840 standards, with an effective orifice area of 2.019 cm^2, a regurgitant fraction of 5.693%, and a transvalvular pressure gradient of 7.576 mmHg. Moreover, the optimized valve maintained its structural integrity and functionality over 14 million cycles of the accelerated wear test, whereas the unoptimized valve failed after two million cycles. These findings confirm that the FEM-based geometric optimization method enhances both the mechanical performance and durability of PHVs.

Graphical abstract

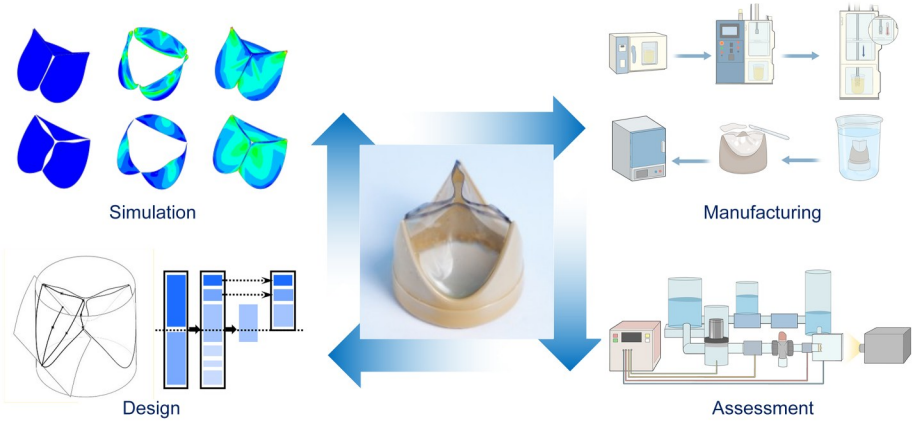

Keywords Polymeric heart valve · Durability · Optimization · Finite element method (FEM) · Dip-molding

✉ Jia Guo
guojia@fudan.edu.cn

✉ Shengzhang Wang
szwang@fudan.edu.cn

[1] Institute of Biomechanics, Department of Aeronautics and Astronautics, Fudan University, Shanghai 200433, China

[2] State Key Laboratory of Molecular Engineering of Polymers, Department of Macromolecular Science, Fudan University, Shanghai 200433, China

[3] Institute of Biomedical Engineering and Technology, Academy for Engineering and Technology, Fudan University, Shanghai 200433, China

1 Introduction

Heart valve disease (HVD) encompasses a group of disorders in which one or more cardiac valves become diseased, leading to abnormal heart function [1]. HVD frequently affects the aortic valve located between the left ventricle and the aorta [2]. Valvular disease is treated with medication, valve repair, and artificial heart valve replacement. The most common types of artificial valves are mechanical heart valves (MHVs) and biological heart valves (BHVs), with a collective surgical replacement rate of approximately 250 000–300 000 procedures per year worldwide [3]. Recent advances in polymer science have led to polymeric heart valves (PHVs) with excellent biocompatibility and biostability. Besides showing encouraging performance in both clinical and preclinical settings [4], PHVs are potentially more durable than BHVs and circumvent the long-term anticoagulation therapy often required after MHV surgery [5–7]. In addition, PHVs can be manufactured with high reproducibility at comparatively low cost through automated processes [8]. However, a limited number of PHVs currently meet the ISO 5840 standard (200 million fatigue cycles) [9], underscoring the need for further durability improvement.

PHVs can be fabricated from various polymers such as polyurethane (PU), polytetrafluoroethylene, and styrene–isobutylene–styrene [10]. PU is especially desirable because its stiffness and flexibility can be tailored to accommodate the dynamic motion of artificial heart valves [9]. For example, the Tria surgical valve (Foldax, USA), formed from silicone PU–urea (LifePolymer), exhibits excellent performance in both in vitro and in vivo experiments [11]. Among the manufacturing processes for PHVs—molding, electrospinning, and additive manufacturing [10]—dip-molding has been popularized as a straightforward and efficient approach [12].

The performance of PHVs can be improved by combining optimal material selection with advanced processing techniques. For instance, applying injection molding, Stasiak et al. [13] fabricated anisotropic PHVs with mechanical properties exceeding the ISO requirements. Combining impregnation coating, four-axis three-dimensional (3D) printing, and different grades of elastic PU, Giaretta et al. [14] produced structurally reinforced PHVs. Chen et al. [15] introduced a durable composite material comprising a soft polymer matrix and knitted fabric for polymeric valves. However, valve function depends not only on the material and fabrication process, but also on the geometric configuration of the valve [16]. Kuan et al. [17] showed that the mechanical efficiency, orifice area, and stress distribution were improved in tri-leaflet valves. Burriesci et al. [18] numerically optimized valve designs using finite element analysis and Xu et al. [19] constructed a parameterized leaflet morphology using edge surfaces and splines, providing a valuable foundation for design optimization based on the movement of control points. Despite these advances, few investigations have attempted to improve the PHV durability through geometric optimization.

The present study introduces a PU material suitable for PHVs and establishes a comprehensive finite element method (FEM)-based framework for finding the geometric configuration that optimizes the mechanical performance of PHVs. A novel integrated impregnation processing device is also designed. Valve samples with different geometries—both before and after optimization—were fabricated and evaluated through in vitro pulsatile-flow testing and fatigue experiments. This work offers a feasible approach for enhancing the durability of polymeric valves through advanced geometric optimization.

2 Materials and methods

2.1 Materials

The PU material was a typical multiblock copolymer containing soft and hard segments, synthesized as previously reported [11, 20]. The reaction conditions and composition were modified (specifically, we exchanged poly(hexamethylene oxide) (PHMO) with poly(tetrahydrofuran) because PHMO is commercially unavailable) to fabricate PU materials that meet the property requirements of implantable heart valve leaflets (LifePolymer, Foldax, USA [11]). The soft segment consisted of a poly(tetrahydrofuran) block (PTMG, 20% mass fraction) and an α,ω-bis(6-hydroxyethoxypropyl) polydimethylsiloxane block (PDMS, 80% mass fraction), using methylene diphenyl diisocyanate (MDI) as the chain extender (Fig. 1a). The hard segment was a copolymer of MDI with 1,3-bis(4-hydroxybutyl)-1,1,3,3-tetramethyldisiloxane (BHTD) and ethylenediamine (EDA), forming mixed urea and urethane bonds. The proportions of hard and soft segments in the resulting product (TSPEUU) were 45% and 55% (mass fraction), respectively.

2.1.1 Synthesis of TSPEUU

The specified contents of PTMG and PDMS were placed in a 100-mL round-bottomed flask and dried under a vacuum at 105 °C for 1.5 h. The resulting mixture was cooled to 75 °C, and the flask was charged with nitrogen. MDI was added to the mixture with mechanical stirring. After 30 min of reaction, BHTD was added, and the reaction was continued for a further 2 h. Afterwards, the mixture was cooled to room temperature and then retained in an ice bath. EDA was added dropwise through a micropump for chain extension. This reaction continued for 30 min at 85 °C with stirring. Finally, the residual isocyanate groups were reacted with anhydrous alcohol for end-capping.

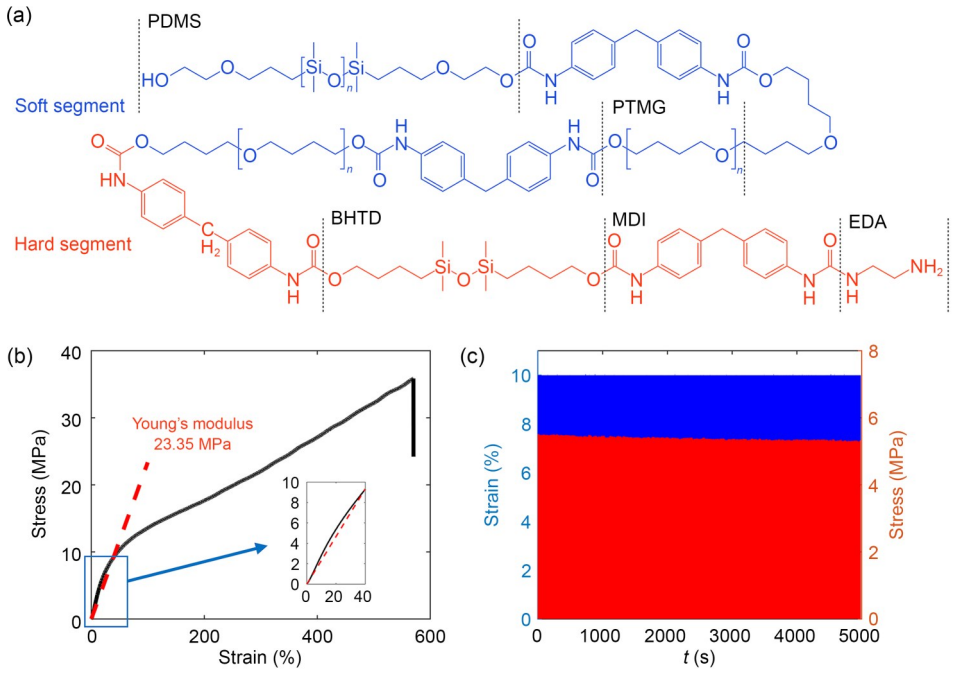

Fig. 1 Chemical formula (a) and uniaxial tensile test results (b) of TSPEUU. (c) Dynamic fatigue test results of TSPEUU under constant displacement

2.1.2 Mechanical properties of TSPEUU film

A TSPEUU film with an approximate thickness of 0.4 mm was prepared on a polypropylene mold via an impregnation film-forming route. Replicate ISO 37 type 3 dumbbell specimens were cut from the film for mechanical testing. Subsequently, static uniaxial tensile tests were conducted at 20 mm/min on specimens with an initial length of 16 mm. The stress–strain relationship of TSPEUU (Fig. 1b) was approximately linear during the early stage (below 40% strain, the main strain range of the PHV in this study). The Young's modulus and ultimate tensile strength were 23.35 and 35.87 MPa, respectively, and the elongation at break was approximately 570%. Dynamic fatigue tensile tests were performed on three batches of samples under constant strain. The stress loss remained at (–3.46±0.45)% under the test conditions, confirming the stable fatigue resistance of TSPEUU. As shown in Fig. 1c, the representative TSPEUU film lost 3.46% of its stress after 50 000 cycles at 10 Hz under 10% strain (see Fig. S1 in the supplementary information for the results of repeated experiments).

2.2 Methods

2.2.1 Parametric design of the leaflet

To design the geometric configuration of the tri-leaflet polymeric valve under stress-free conditions, we specified three fundamental curves: the boundary edge, the free edge, and the belly curve [21]. Each curve was defined with B-spline functions (Fig. 2). The overall valve geometry was controlled by seven variable parameters: the y and z coordinates of the control points of the belly and boundary curves, the valve height, the gap between the leaflet and central axis, and the gap between adjacent leaflets. The valve diameter was fixed at 25 mm [22]. The ranges of the seven parameters are listed in Table 1.

2.2.2 Finite-element-based optimization framework of the polymeric aortic valve

The geometric leaflet model was imported into ABAQUS 2022 (Dassault Systèmes, France) for FEM simulation. The dynamic leaflet behavior was analyzed under a transvalvular pressure gradient. The boundary edge of the leaflet was fully constrained [23], and the physiological dynamic loading condition was defined by the transvalvular pressure gradient curve observed in normal human aortic valves [24]. The load was applied perpendicularly to the ventricular-facing surface of the polymeric aortic valve (red surface in Fig. 3a). The corresponding transvalvular pressure profile is shown in Fig. 3b. The leaflet was treated as a linear elastic material with Young's modulus of 23.35 MPa and Poisson's ratio of 0.3. The meshing (approximately 1500 elements) was completed in ABAQUS. The elements were shell elements with a thickness of 0.2 mm. The mechanical equilibrium equations were solved with an explicit solver under the quasi-static assumption, ensuring that the ratio of kinetic energy to internal energy remained below 5% [25]. To streamline the analysis of multiple design parameters, the

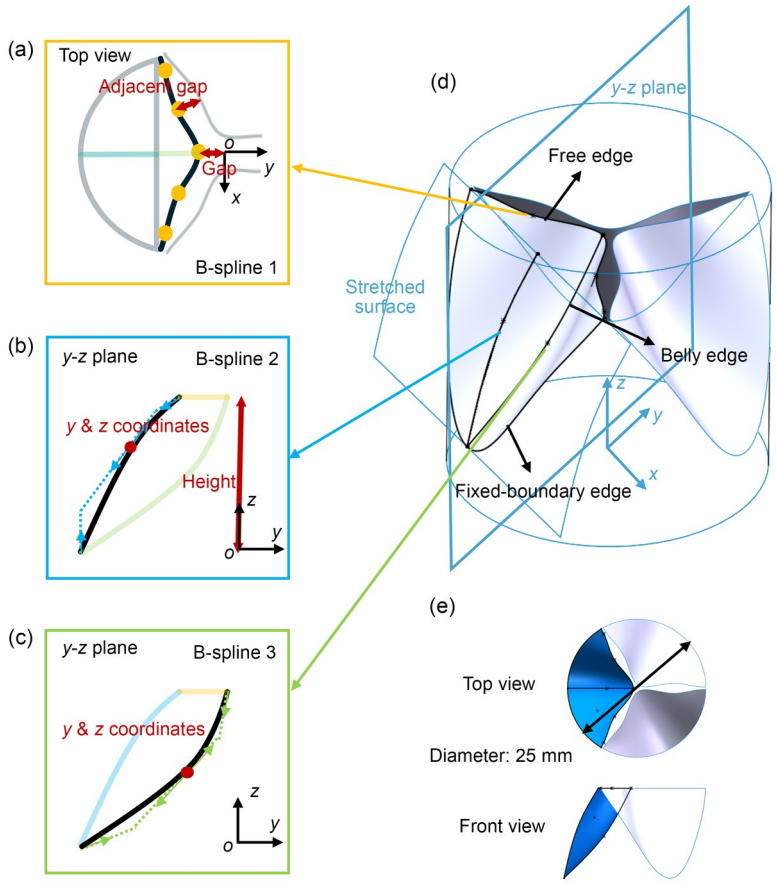

Fig. 2 Geometric configuration of the tri-leaflet polymeric valve: (a) free edge with five control points and two variable parameters; (b) fixed-boundary edge, on which the morphology is influenced by the second B-spline functions characterized by one control point and two variable parameters; (c) belly edge with one control point and two variable parameters; (d) overall geometric morphology and drawing process of the valve; (e) top and front views of the valve

Table 1 Parameter ranges in the parametric design of the leaflet

Parameter	Lower bound (mm)	Upper bound (mm)
Height	14	16
Gap	0.2	1
Leaflet gap	0.5	1.5
y-coordinate of the control point of the belly curve	–8	–4
z-coordinate of the control point of the belly curve	5	9
y-coordinate of the control point of the boundary curve	–12	–8
z-coordinate of the control point of the boundary curve	5	9

Gap refers to the gap between the leaflet and central axis; Leaflet gap refers to the gap between adjacent leaflets

simulation process was automated using an ABAQUS Python script [26].

The valve geometry was optimized using the non-dominated sorting genetic algorithm II (NSGA-II) [27]. The optimization objectives were the maximum stress and mean stress of the total volume and time, and the geometric scale factor (GSF) determining the degree of valve opening. The GSF (Fig. 4) is computed as follows:

$$\mathrm{GSF} = (S_1 - S_2)/S_1,$$

where S_1 and S_2 denote the leaflet face area at the maximum opening and the closing, respectively. The GSF is large when the valve is widely opened, and it decreases as the valve closes. The main parameters of the employed NSGA-II algorithm—population size, number of generations, crossover probability, crossover distribution index, and mutation distribution index—are listed in Table 2. First, a preliminary optimization result was obtained under setting No. 1 in Table 2. Inspired by Ref. [21], the initial valve shape was small with a height, gap, and leaflet gap of 15 mm, 1 mm, and 1 mm, respectively.

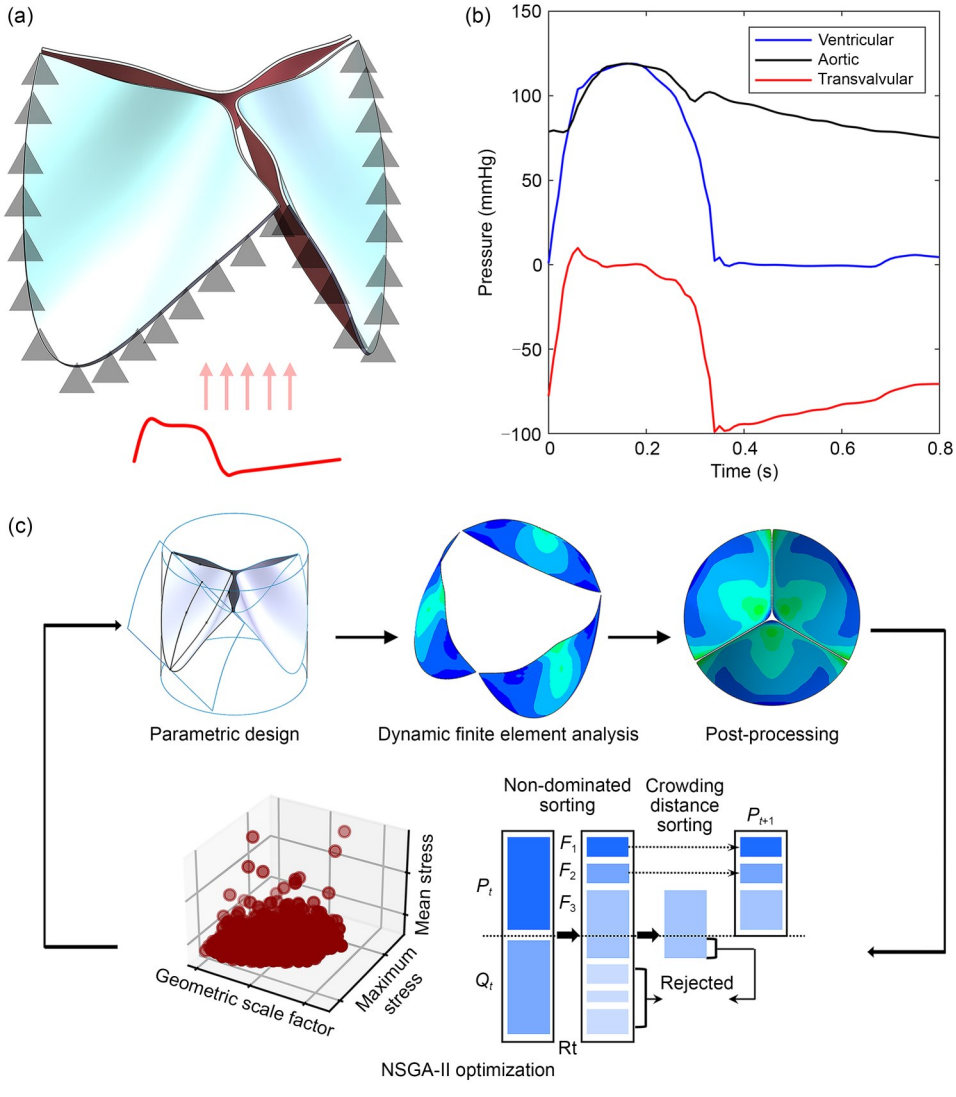

Fig. 3 Finite-element-based optimization framework of the polymeric aortic valves. (a) Schematic of the finite element simulation conditions. (b) Transvalvular pressure curve of the aortic valve in a normal human heart. (c) Geometric optimization platform for designing polymer heart valves based on finite element simulation. 1 mmHg=133 Pa

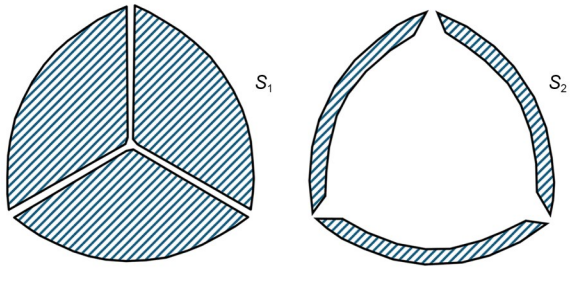

Fig. 4 Schematic showing the geometric scale factor (GSF) of the valve

The *y*-*z* coordinates were (−6.750 mm, 7.500 mm) for the control point of the belly curve and (−9.375 mm, 7.500 mm) for the control point of the boundary curve. The initially optimized result was substituted into the larger-size No. 2 setting to calculate the final optimized valve geometry. The FEM-based geometric optimization process of the PHV is shown in Fig. 3c.

Among the Pareto fronts derived through the optimization process [28], the parameter set associated with the lowest maximum stress was selected as the final optimized configuration. The valve geometries before and after optimization were compared in terms of their Gaussian and mean curvatures [29].

Table 2 Parameters of the NSGA-II algorithm

Parameter	No. 1	No. 2
Population size	12	40
Number of generations	20	120
Crossover probability	0.9	0.8
Crossover distribution index	10	8
Mutation distribution index	20	15

2.2.3 Dip-molding apparatus for fabricating the polymer artificial heart valve

The artificial PHVs were fabricated in a dip-molding apparatus developed by our group. The overall process is illustrated in Fig. 5. Both the TSPEUU DMAc solution (0.25 g/mL) and the apparatus were first pre-heated. The mold, stent (leaflet support), and mold with the mounted stent were then sequentially immersed in the solution, ensuring a smooth transition and natural adhesion between the leaflet and support [30, 31]. This process yielded an integrally formed polymeric valve incorporating both the leaflet and the stent. The assembly and its mold were subsequently immersed in water for demolding. The demolded valve was trimmed to the desired leaflet geometry using a scalpel and placed in a vacuum drying oven for final drying. The valve stents were obtained by cutting rods of polyether ether ketone (having similar mechanical properties to Tria [11]) using computer numerical control machining, and their structures were contoured to the boundary edge shape of the valves. The valve stents were 0.5-mm thick.

2.2.4 In vitro hydrodynamic assessment

The hemodynamic performances of the fabricated valves were evaluated in an in vitro pulsatile-flow test system that complies with ISO 5840 standards [32]. The mean arterial pressure, heart rate, cardiac output, and systolic-phase proportion were 100 mmHg (1 mmHg=133 Pa), 75 beats per minute (bpm), 5 L/min, and 35%, respectively. The working fluid was 0.9% (9 g/L) saline at 37 °C. The primary hemodynamic parameters were the effective orifice area (EOA), transvalvular pressure gradient, and regurgitant fraction. The EOA (denoted as A_{eo}, in cm^2) is calculated from the flow and pressure or velocity data as follows:

$$A_{eo} = \frac{qv_{RMS}}{51.6 \times \sqrt{\frac{\Delta p}{\rho}}},$$

where qv_{RMS} (mL/s) is the root-mean-square of the forward flow during the positive-pressure differential period, ρ is the fluid density, and Δp (mmHg) is the mean pressure differential measured during the positive-pressure phase [22]. To validate the numerical simulation, the agreement between the valve motion observed in the pulsatile-flow experiments and the corresponding predicted motion was quantified by the Dice coefficient s [33], calculated as

$$s = \frac{2|X \cap Y|}{|X| + |Y|},$$

where $X \cap Y$ represents the intersection between samples X and Y, and $|X|$ and $|Y|$ denote the numbers of elements in X and Y, respectively. The numerator is doubled because the denominator involves the repeated counting of elements common to X and Y. In this study, X and Y represent the opening areas at the center of the valve in the simulation results and the pulsatile-flow test results, respectively. The valve durability was evaluated through accelerated wear tests [34] at 900–1200 bpm in 9 g/L saline at 37 °C. According to the ISO 5840-3 standard, the number of cycles was recorded at each instance of valve opening and closing. During testing, it was ensured that the maximum pressure differential exceeded 95 mmHg when the valve was closed, and that the pressure exceeded this threshold for more than 5% of the time in each cycle.

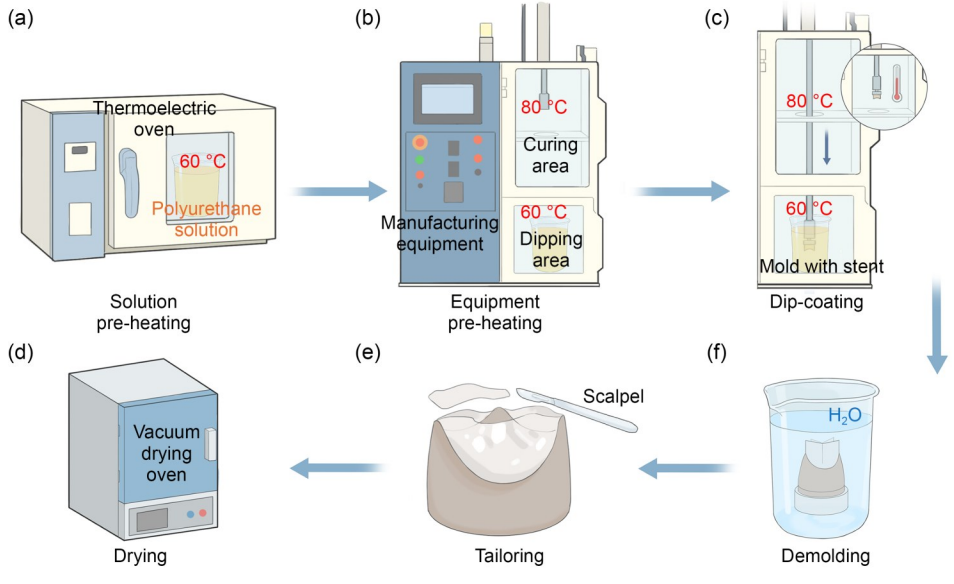

Fig. 5 Process flow of polymer valve dip-molding: (a) pre-heating of the polyurethane solution; (b) pre-heating of the dip-molding equipment; (c) dip-molding process; (d) drying process of the finished valves; (e) trimming of excess material; (f) demolding process

3 Results

3.1 Design results

Figures 6a and 6b display the geometric configurations of the valves before and after optimization, respectively. The magnitude distributions of the Gaussian and mean curvatures of the valve leaflets, obtained only for the configurations before and after optimization, are shown in Figs. 6d and 6e. Both configurations showed similar mean curvature distributions with a comparable overall bending trend, but different intrinsic surface features. In particular, the regions of negative Gaussian curvature were enlarged in the optimized design, revealing localized changes in the bending direction from those in the pre-optimized configuration. Figures 6c and 6f display the evolutions of the three fundamental curves (boundary edge, belly curve, and free edge) in all configurations during the optimization process. In the side view of the optimized configuration (Fig. 6c), the boundary edge approximated a straight line, the belly curve was concave, and the free edge showed slight undulations.

3.2 Results of the finite element method

The historical distributions of the three optimization objectives (maximum stress, mean stress, and GSF), the Pareto front of the optimization results, and the corresponding optimal points are displayed in Figs. 7a and 7f. The mean maximum stress, mean stress, and GSF values of the optimization results were (2.3221±0.2799) MPa, (0.5105±0.0275) MPa, and 0.8439±0.0506, respectively. In the finally optimized result, maximum stress was minimized at 1.7773 MPa during a single cardiac cycle, the GSF was relatively high (0.8138), and mean stress was relatively low (0.4888 MPa). Notably, these optimized results lie on the Pareto front in both the mean stress−maximum stress and GSF−maximum stress planes, confirming the reliability of the optimization procedure.

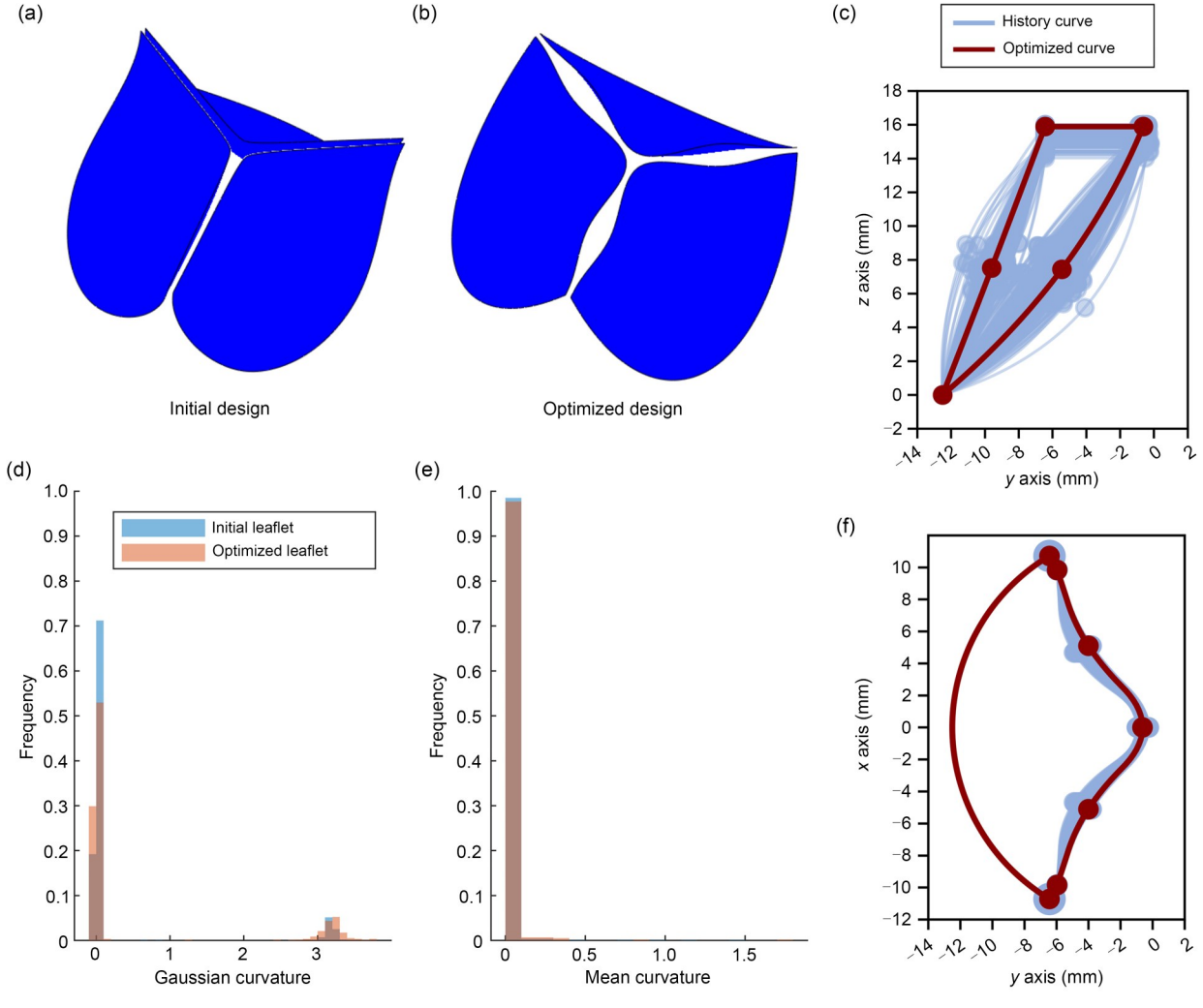

Fig. 6 Valve-geometry optimization results. Initial (a) and optimized (b) valve designs. (c) Right-side view of the valve-optimization history. Histograms of Gaussian curvature (d) and mean curvature (e) distributions on the valve surface. (f) Top view of the valve-optimization history

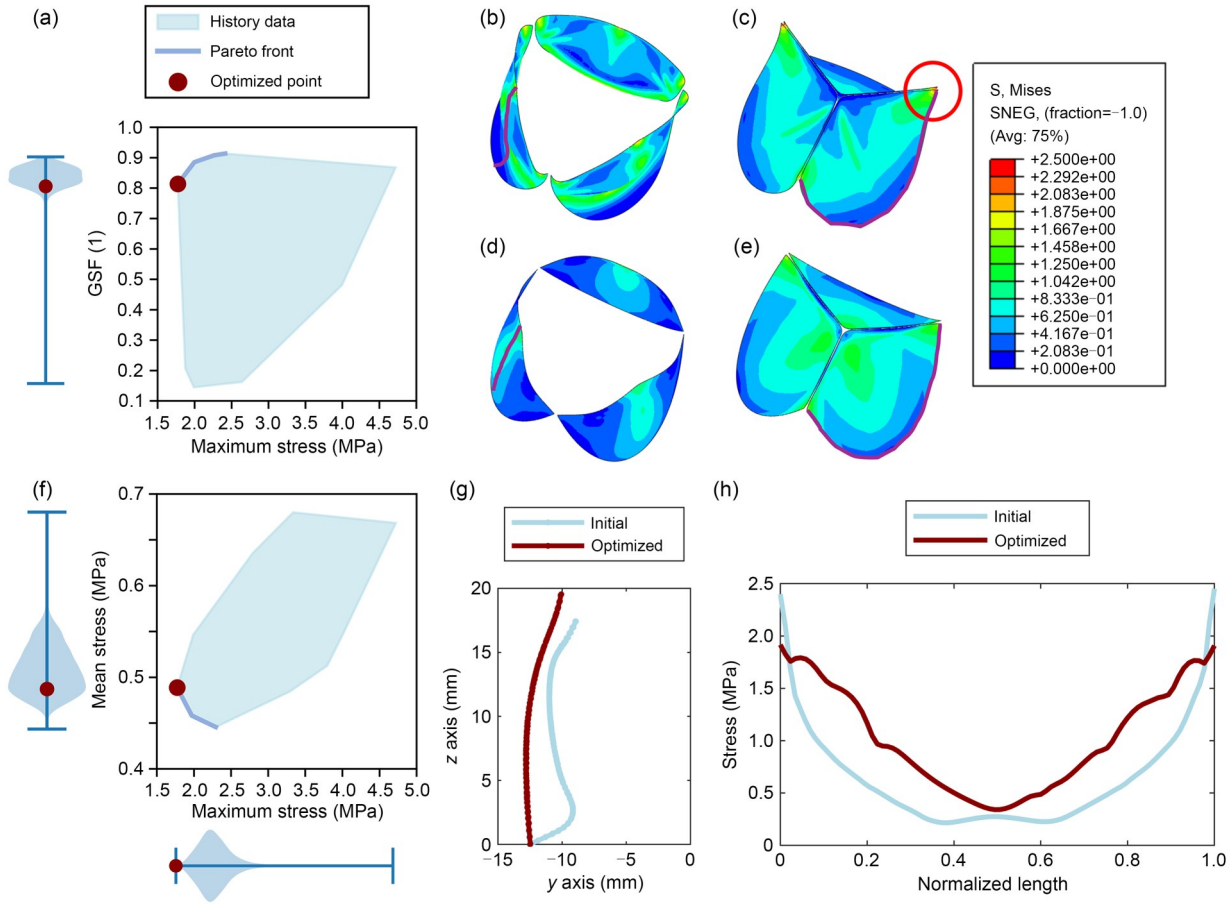

Fig. 7 FEM results. (a) FEM results on the maximum stress–GSF plane. Stress distributions of the maximally opened (b) and fully closed (c) pre-optimized valve. Stress distributions of the maximally opened (d) and fully closed (e) optimized valve. (f) FEM results on the maximum stress–mean stress plane. (g) Deformed belly edges of the maximally opened valve before and after optimization. (h) Stress distributions along the boundary edge of the valve before and after optimization

Figures 7b–7e present the stress-distribution contour maps of the pre-optimized and optimized valves when maximally opened and fully closed. In the pre-optimized configuration, the stress was maximized at 2.4802 MPa during the diastolic phase (when the valve was closed), specifically, at the terminal region of the attachment edge (highlighted by the red circle in Fig. 7c). Moreover, the pre-optimized valve exhibited obvious bending in the boundary edge region during opening. To further illustrate the geometric improvements of the optimized design, Fig. 7g plots the belly curves (purple curves in Figs. 7b and 7d) after extracting the element nodes near the belly curve at the time points of maximum opening of the pre-optimized and optimized valves. The optimized valve presented a flatter belly curve than its pre-optimized counterpart. Figure 7h shows the stress distributions along the boundary edges (purple curves in Figs. 7c and 7e) during valve closure, when the transvalvular pressure differential was maximized. After optimization, the stress along the boundary edge became more uniformly distributed, accompanied by a reduced stress range and a lower maximum stress overall.

3.3 Experimental results

The fabricated optimized valve exhibited a smooth, transparent surface (Figs. 8a and 8b), a geometric morphology that aligned with the design specifications, and the intended critical dimensions (such as valve height and diameter). The leaflet thickness was measured at five distinct locations on the pre-optimized and optimized tri-leaflet valves. The average thickness (0.19 mm) closely matched the thickness (0.20 mm) adopted in the simulations, with a numerical deviation of only 5%. This thickness difference did not significantly affect the simulation results of the valves. Notably, the thickness of both valves was highest at position 3, likely resulting from the orientation of the mold during dip-molding and the viscosity of the TSPEUU solution.

Figure 9 presents the pulsatile-flow test results of the valves before and after optimization. The EOAs of the pre-optimized and optimized valves were (1.944±0.011) and (2.019±0.024) cm^2, respectively, both exceeding the ISO 5840 requirement (1.45 cm^2). The EOA increased slightly following optimization. Meanwhile, the regurgitant

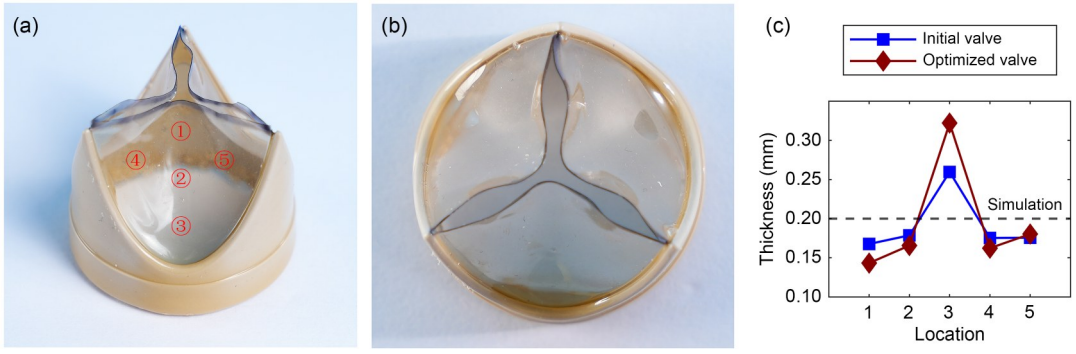

Fig. 8 Finished valves. (a) Photograph of the optimized valve. (b) Photograph of the top view of the optimized valve. (c) Measurement results of valve membrane thickness

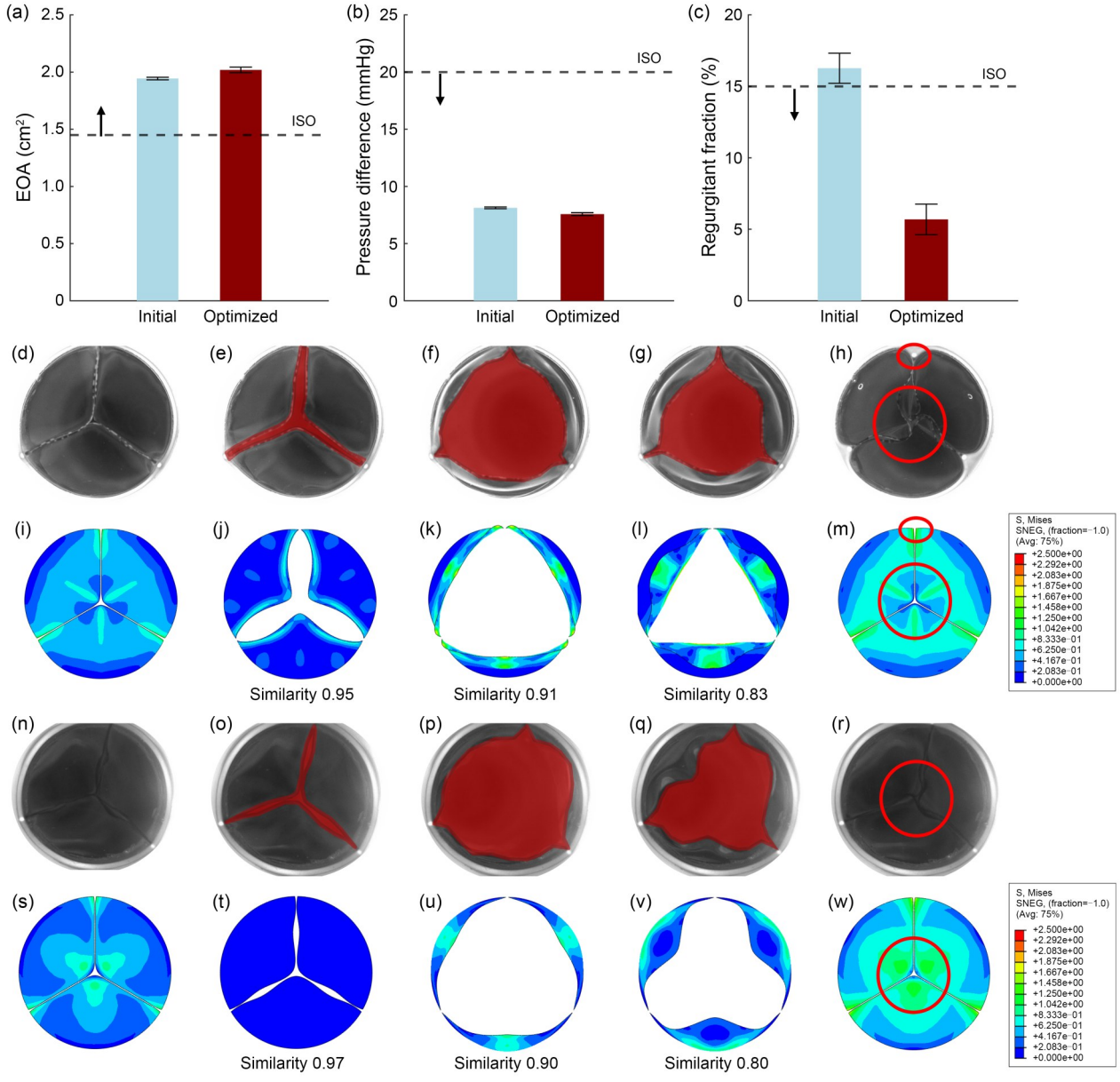

Fig. 9 Results of pulsatile-flow tests and FEM simulations before and after optimization. (a–c) Results of pulsatile-flow tests. Comparisons of valve opening and closing behaviors in the FEM simulations (stress distributions) and pulsatile-flow tests before (d–m) and after (n–w) optimization. 1 mmHg=133 Pa. Data are expressed as mean±standard deviation (n=3)

fraction of the pre-optimized valve ((16.268±1.050)%) failed to meet the ISO threshold (15%). After optimization, the regurgitant fraction was reduced by 65.00% and was well compliant with ISO 5840, reaching (5.693±1.063)% . The mean transvalvular pressure gradients of the pre-optimized and optimized valves were (8.128±0.074) and (7.576± 0.125) mmHg, respectively, both satisfying the ISO 5840 requirement (<20 mmHg) but showing a 6.79% reduction in the optimized valve. Panels e–g, j–l, o–q, and t–v of Fig. 9 compare the opening and closing behaviors of the optimized valve under pulsatile-flow conditions with those of the FEM simulations (stress distributions). The agreement between the experimentally obtained images and the simulation outputs, quantified in terms of the Dice coefficient, yielded similarities above 0.9 during systole and 0.8 during diastole, validating the simulation accuracy.

Figures 10a–10c present the outcomes of the accelerated wear tests. After two million cycles (Fig. 10b), the leaflet of the pre-optimized valve detached from the supporting stent, leading to complete loss of valve function. In contrast, the optimized valve retained its structural and functional integrity beyond 14 million cycles. During pulsatile-flow tests performed both before fatigue tests and after 390 000, 780 000, 1 197 000, and 1 497 000 cycles, the optimized valve consistently met ISO 5840 requirements for EOA, transvalvular pressure gradient, and regurgitant fraction, demonstrating maintained hemodynamic performance throughout the test duration.

4 Discussion

This study presents an integrated design–simulation–manufacturing–assessment approach for optimizing the geometric parameters and hence improving the durability of artificial PHVs.

The geometric configurations markedly differed in the pre-optimized and optimized designs. The variations in curvature distribution across the valve surfaces contributed to the observed performance differences. Notably, slight undulations at the free edge of the optimized valve increased the overall buckling degree of the leaflet [35], facilitating the alignment of stiffness with the dynamic motion of the leaflet [23]. Moreover, the topological features corresponding to the Gaussian curvature of the optimized valve relaxed the geometric motion of the valve (Fig. 7g).

Excessive stress concentration during the cardiac cycle can tear the leaflet (Fig. 10b), compromising the durability of the valve [36]. During optimization, the leaflet geometry was adjusted to reduce the localized stress, thereby improving the long-term performance. In the pre-optimized design, stress was concentrated at the terminal region of the boundary edge during closure, probably causing stent bending and leaflet detachment from the stent (Figs. 9h and 10b). Consequently, the valve was incompletely closed and the regurgitant fraction was raised. In contrast, the stress was uniformly distributed at the center of the optimized valve during closure

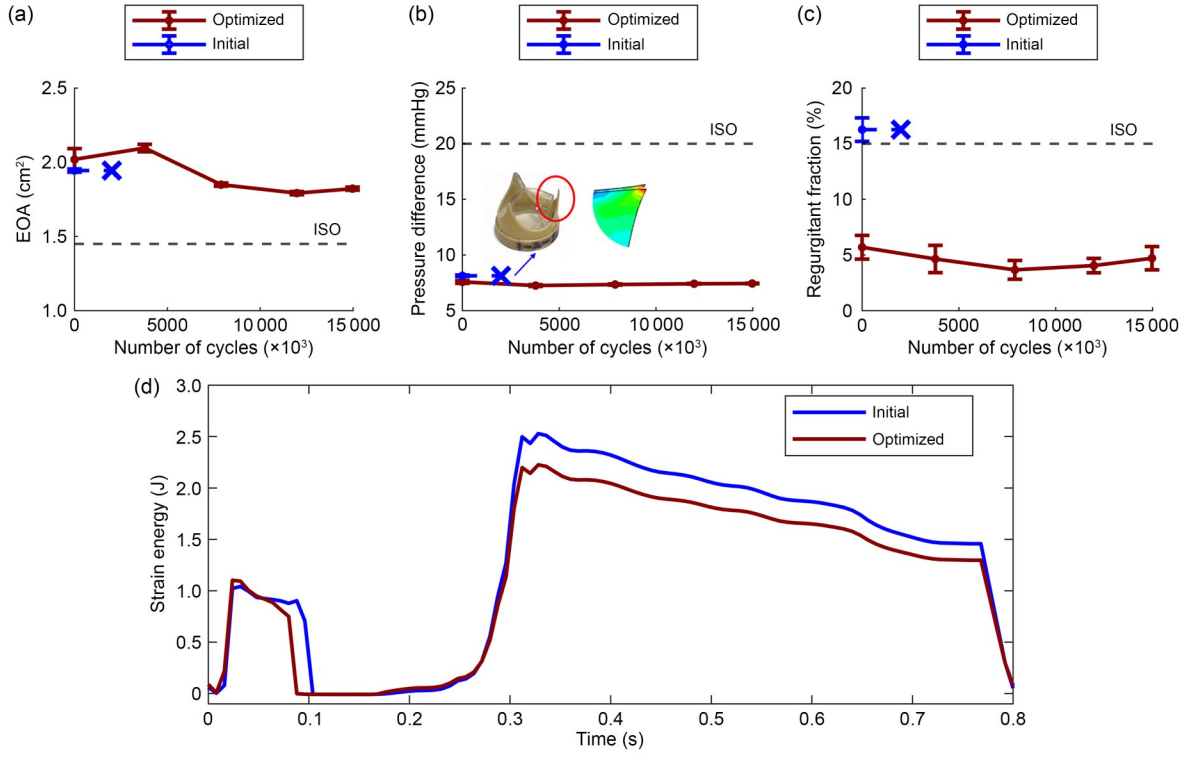

Fig. 10 Results of the pulsatile-flow tests after the accelerated wear testing of the valves over one cardiac cycle: (a) EOA; (b) pressure difference; (c) regurgitation fraction; (d) strain energy

(Figs. 9m and 9w). The reduced leaflet redundancy (Fig. 9r) significantly lowered the regurgitant fraction.

The mean stress reflects the overall force imposed on the leaflet. With its lower and more evenly distributed mean stress, the optimized valve was more durable than the pre-optimized valve. The strain energy throughout the cardiac cycle was also lowered in the optimized valve (Fig. 10d), further enhancing the durability because less energy was expended during valve opening and closing.

The membrane thickness of the valve is affected by various factors of the manufacturing process, such as the concentration of polymer solution, the mold and solution temperatures, the impregnation speed, the duration of staying in solution, and the number of impregnations [37]. In this study, these experimental conditions were determined through pre-experiments. The average membrane thickness of the valve was controlled at 0.19 mm, only 5% lower than the simulation value (0.20 mm). The membrane thickness, which influences the valve performance, may vary within approximately 50% in the same valve leaf, even when all factors are well controlled [38]. This study investigated only the effect of geometric shape on valve performance. Future research will explore the effects of valve thickness and its distribution.

Whereas most studies have enhanced the durability through material design and fabrication processes [13,15], this study demonstrated that geometric optimization can largely improve the mechanical performance, hemodynamic characteristics, and overall durability of polymeric aortic valves. Nonetheless, certain limitations remain. The complex physiological environment in vivo cannot be fully replicated during in vitro evaluations and requires further validation. In addition, both the optimization framework and the dip-molding platform must adapt to different heart valve types and sizes, necessitating future scalability and generalizability investigations. For instance, some novel machine learning algorithms could be incorporated into the optimization framework, and the dip-molding platform could be combined with 3D printing. By incorporating a simulation of fluid–structure interactions, we could refine the applied pressure on the leaflet surface and improve the membrane-thickness control during dip-molding, thus enhancing the precision and applicability of our approach.

5 Conclusions

This study presents an integrated design–simulation–manufacturing–assessment approach for the geometric optimization of artificial PHVs. Following optimization, the valve stress was more uniformly distributed throughout the cardiac cycle, and the maximum stress was reduced by 28.34% (from 2.4802 MPa in the pre-optimized valve to 1.7773 MPa). The optimized valve also demonstrated a more relaxed opening state than the pre-optimized valve. Pulsatile-flow testing confirmed that the EOA, transvalvular pressure gradient, and regurgitant fraction of the optimized valve meet the ISO standards. The regurgitant fraction was 5.693%, 65% lower than the pre-optimized value. Furthermore, during accelerated wear testing, the optimized valve sustained 14 million cycles, seven times the cycle number withstood by the pre-optimized valve.

In summary, this work provides an effective methodology and theoretical framework for designing and fabricating polymeric aortic valves, highlighting that geometric optimization can feasibly enhance the performance of PHVs. Future efforts will focus on further refinement of the optimization model and manufacturing processes to advance the clinical translation of polymeric valves, ultimately benefiting a broad population of patients with HVD.

Supplementary Information The online version contains supplementary material available at https://doi.org/10.1631/bdm.2500046.

Acknowledgements This work was partially funded by the National Natural Science Foundation of China (No. 82400370) and the Interdisciplinary Innovation Team Incubation Project of Children's Hospital of Fudan University (No. EKYX202416).

Author contributions TLX: methodology, simulation, experiments, result analysis, writing—original draft, and writing—review & editing. ZHZ: material synthesis, experiments, writing—original draft, and writing—review & editing. YHC: simulation and experiments. SPC: material design, synthesis, experiments, and writing—original draft. JG: writing—review & editing, conceptualization, and resources. SZW: writing—review & editing, conceptualization, resources, funding acquisition, supervision, and project administration.

Declarations

Conflict of interest The authors declare that they have no conflict of interest.

Ethical approval This article does not contain any studies with human or animal subjects performed by any of the authors.

Data availability The data that support the findings of this study are available from the corresponding authors upon reasonable request.

References

1. Williams JK, Yoo JJ, Atala A (2019) Regenerative medicine approaches for tissue engineered heart valves. In: Atala A, Lanza R, Mikos AG et al (Eds.), Principles of Regenerative Medicine (3rd Ed.). Elsevier, p.1041–1058. https://doi.org/10.1016/b978-0-12-809880-6.00059-x
2. Coffey S, Roberts-Thomson R, Brown A et al (2021) Global epidemiology of valvular heart disease. Nat Rev Cardiol 18(12): 853–864. https://doi.org/10.1038/s41569-021-00570-z
3. Rezvova MA, Klyshnikov KY, Gritskevich AA et al (2023) Polymeric heart valves will displace mechanical and tissue heart valves: a new era for the medical devices. Int J Mol Sci 24(4):

3963.
https://doi.org/10.3390/ijms24043963
4. Resor CD, Bhatt DL (2019) Polymeric heart valves: back to the future? Matter 1(1):30–32.
https://doi.org/10.1016/j.matt.2019.06.003
5. Arcidiacono G, Corvi A, Severi T (2005) Functional analysis of bioprosthetic heart valves. J Biomech 38(7):1483–1490.
https://doi.org/10.1016/j.jbiomech.2004.07.007
6. Dangas GD, Weitz JI, Giustino G et al (2016) Prosthetic heart valve thrombosis. J Am Coll Cardiol 68(24):2670–2689.
https://doi.org/10.1016/j.jacc.2016.09.958
7. de Kort BJ, Koch SE, Wissing TB et al (2021) Immunoregenerative biomaterials for in situ cardiovascular tissue engineering – do patient characteristics warrant precision engineering? Adv Drug Deliv Rev 178:113960.
https://doi.org/10.1016/j.addr.2021.113960
8. Singh SK, Kachel M, Castillero E et al (2023) Polymeric prosthetic heart valves: a review of current technologies and future directions. Front Cardiovasc Med 10:1137827.
https://doi.org/10.3389/fcvm.2023.1137827
9. Wu Y, Zhou J, Li T et al (2024) A review of polymeric heart valves leaflet geometric configuration and structural optimization. Comput Methods Biomech Biomed Engin (early access).
https://doi.org/10.1080/10255842.2024.2410232
10. Oveissi F, Naficy S, Lee A et al (2019) Materials and manufacturing perspectives in engineering heart valves: a review. Mater Today Bio 5:100038.
https://doi.org/10.1016/j.mtbio.2019.100038
11. Jenney C, Millson P, Grainger DW et al (2021) Assessment of a siloxane poly(urethane-urea) elastomer designed for implantable heart valve leaflets. Adv NanoBiomed Res 1(2):2000032.
https://doi.org/10.1002/anbr.202000032
12. Li RL, Russ J, Paschalides C et al (2019) Mechanical considerations for polymeric heart valve development: biomechanics, materials, design and manufacturing. Biomaterials 225:119493.
https://doi.org/10.1016/j.biomaterials.2019.119493
13. Stasiak JR, Serrani M, Biral E et al (2020) Design, development, testing at ISO standards and in vivo feasibility study of a novel polymeric heart valve prosthesis. Biomater Sci 8(16):4467–4480.
https://doi.org/10.1039/d0bm00412j
14. Giaretta J, Crago M, Hoang TP et al (2024) Structural reinforcements as a strategy toward durable polymeric heart valves. Cell Rep Phys Sci 5(3):101870.
https://doi.org/10.1016/j.xcrp.2024.101870
15. Chen X, Liu FK, Yu QF et al (2025) A soft and fatigue-resistant material that mimics heart valves. Matter 8(2):101926.
https://doi.org/10.1016/j.matt.2024.11.020
16. Wojciechowska D, Liberski AR, Wilczek P et al (2017) The optimal shape of an aortic heart valve replacement – on the road to the consensus. Qscience Connect 2017(3):1.
https://doi.org/10.5339/connect.2017.1
17. Kuan YH, Dasi LP, Yoganathan A et al (2011) Recent advances in polymeric heart valves research. Int J Biomater Res Eng 1(1):1–17.
https://doi.org/10.4018/ijbre.2011010101
18. Burriesci G, Marincola FC, Zervides C (2010) Design of a novel polymeric heart valve. J Med Eng Technol 34(1):7–22.
https://doi.org/10.3109/03091900903261241
19. Xu F, Morganti S, Zakerzadeh R et al (2018) A framework for designing patient-specific bioprosthetic heart valves using immersogeometric fluid-structure interaction analysis. Int J Numer Method Biomed Eng 34(4):e2938.
https://doi.org/10.1002/cnm.2938
20. Dandeniyage LS, Adhikari R, Bown M et al (2019) Morphology and surface properties of high strength siloxane poly(urethane-urea)s developed for heart valve application. J Biomed Mater Res B Appl Biomater 107(1):112–121.
https://doi.org/10.1002/jbm.b.34101
21. Abbasi M, Azadani AN (2020) A geometry optimization framework for transcatheter heart valve leaflet design. J Mech Behav Biomed Mater 102:103491.
https://doi.org/10.1016/j.jmbbm.2019.103491
22. ISO 5840-1 (2021) Cardiovascular Implants—Cardiac Valve Prostheses-Part 1: General Requirements. ISO
23. Smid CC, Pappas GA, Cesarovic N et al (2024) Novel heart valve leaflet designs with stiff polymeric materials and biomimetic kinematics. Bio-Des Manuf 7(6):1018–1034.
https://doi.org/10.1007/s42242-024-00309-y
24. Khonsary SA (2017) Guyton and Hall: textbook of medical physiology. Surg Neurol Int 8:275.
https://doi.org/10.4103/sni.sni_327_17
25. Smith M (2009) ABAQUS/Standard User's Manual, Version 6.9. Dassault Systèmes Simulia Corp.
https://research.manchester.ac.uk/en/publications/abaqusstandard-users-manual-version-69 [Accessed on 30 October 2023]
26. Yuan J, Si JH, Qiao Y et al (2024) Parametric modeling and numerical simulation of a three-dimensional random aggregate model of lime–sand piles based on Python–Abaqus. Buildings 14(6):1842.
https://doi.org/10.3390/buildings14061842
27. Deb K, Pratap A, Agarwal S et al (2002) A fast and elitist multiobjective genetic algorithm: NSGA-II. IEEE Trans Evol Comput 6(2):182–197.
https://doi.org/10.1109/4235.996017
28. Mueller-Gritschneder D, Graeb H, Schlichtmann U (2009) A successive approach to compute the bounded Pareto front of practical multiobjective optimization problems. SIAM J Optim 20(2):915–934.
https://doi.org/10.1137/080729013
29. Banchoff TF, Lovett S (2023) Differential Geometry of Curves and Surfaces (3rd Ed.). CRC Press, New York, USA.
https://doi.org/10.1201/9781003295341
30. Leat ME, Fisher J (1995) The influence of manufacturing methods on the function and performance of a synthetic leaflet heart valve. Proc Inst Mech Eng H 209(1):65–69.
https://doi.org/10.1243/pime_proc_1995_209_318_02
31. Boffito M, Sartori S, Mattu C et al (2016) Polyurethanes for cardiac applications. In: Cooper SL, Guan JJ (Eds.), Advances in Polyurethane Biomaterials (1st Ed.). Elsevier, p.387–416.
https://doi.org/10.1016/b978-0-08-100614-6.00013-5
32. ISO 5840-2 (2021) Cardiovascular Implants—Cardiac Valve Prostheses-Part 2: Surgically Implanted Heart Valve Substitutes. ISO
33. Dice LR (1945) Measures of the amount of ecologic association between species. Ecology 26(3):297–302.
https://doi.org/10.2307/1932409
34. Raghav V, Okafor I, Quach M et al (2016) Long-term durability of carpentier-edwards magna ease valve: a one billion cycle in vitro study. Ann Thorac Surg 101(5):1759–1765.
https://doi.org/10.1016/j.athoracsur.2015.10.069
35. Calladine CR (1995) Understanding imperfection-sensitivity in the buckling of thin-walled shells. Thin Walled Struct 23(1–4):215–235.
https://doi.org/10.1016/0263-8231(95)00013-4
36. Martin C, Sun W (2014) Simulation of long-term fatigue damage in bioprosthetic heart valves: effects of leaflet and stent elastic properties. Biomech Model Mechanobiol 13(4):759–770.
https://doi.org/10.1007/s10237-013-0532-x
37. Masheane R, Combrinck J, Masheane L (2023) Development of a compression moulding process for the manufacturing of artificial polymer heart valves. In: 24th Annual International RAPDASA Conference Joined by RobMech, PRASA and AMI, Article 06002.
https://doi.org/10.1051/matecconf/202338806002
38. Rahmani B, Tzamtzis S, Ghanbari H et al (2012) Manufacturing and hydrodynamic assessment of a novel aortic valve made of a new nanocomposite polymer. J Biomech 45(7):1205–1211.
https://doi.org/10.1016/j.jbiomech.2012.01.046